

Contents lists available at ScienceDirect

#### Petroleum Science

journal homepage: www.keaipublishing.com/en/journals/petroleum-science



#### Original Paper

# Target-oriented *Q*-compensated reverse-time migration by using optimized pure-mode wave equation in anisotropic media



Shi-Gang Xu a, b, \*, Qian-Zong Bao a, b, Zhi-Ming Ren a, b

- <sup>a</sup> Chang'an University, School of Geological Engineering and Geomatics, Department of Geophysics, Xi'an, Shaanxi, 710064, China
- <sup>b</sup> National Engineering Research Center of Offshore Oil and Gas Exploration, Beijing, 100028, China

#### ARTICLE INFO

# Article history: Received 30 May 2022 Received in revised form 28 September 2022 Accepted 29 December 2022 Available online 6 January 2023

Edited by Jie Hao

Keywords: Anisotropy Attenuation Reverse-time migration Wave equation Optimized algorithm Target-oriented

#### ABSTRACT

Research on seismic anisotropy and attenuation plays a significant role in exploration geophysics. To enhance the imaging quality for complicated structures, we develop several effective improvements for anisotropic attenuation effects in reverse-time migration (O-RTM) on surface and vertical seismic profiling (VSP) acquisition geometries. First, to suppress pseudo-shear wave artifact and numerical instability of the commonly used anisotropic pseudo-acoustic wave equations, an optimized pure P-wave dispersion relation is derived and the corresponding pure-mode wave equation is solved by combining the finite-difference and Possion methods. Second, a simplified anisotropic pure-mode visco-acoustic wave equation (PVAWE) based on standard linear solid model is established. Third, a time-dispersion correlation strategy is applied to improve the modeling accuracy. Fourth, we extend a target-oriented scheme to anisotropic attenuated modeling and imaging. Instead of the conventional wavefield modeling and RTM, the proposed approach can extract available wavefield information near the target regions and produce high imaging resolution for target structures. Last, both anisotropic surface and VSP Q-RTMs are executed by combining optimized PVAWE, time-dispersion correlation and target-oriented algorithm. Modeling examples demonstrate the advantages of our schemes. Moreover, our modified Q-compensated imaging workflow can be regarded as a supplement to the classical anisotropic RTM. © 2023 The Authors, Publishing services by Elsevier B.V. on behalf of KeAi Communications Co. Ltd. This is an open access article under the CC BY-NC-ND license (http://creativecommons.org/licenses/by-nc-nd/ 4.0/).

#### 1. Introduction

In exploration seismology, conventional seismic imaging methods based on the isotropic elastic assumption are not always suitable because of the existence of seismic anisotropy and attenuation in underground media. When directly applying isotropic wave equations for reverse-time migration (RTM) in anisotropic attenuation media, it may give rise to malposed imaging profiles and low resolution of the geologic targets. Therefore, developing improved imaging schemes based on the seismic anisotropy and attenuation theory are significant. The classical RTM workflow relies on high accuracy wavefield extrapolations for source forward propagation and receiver backward propagation (Baysal et al., 1983; McMechan, 1983). In anisotropic media, which is typically represented by transversely isotropic (TI) cases, acoustic wave equations

are widely used in seismic modeling and imaging because they have higher efficiency, simpler forms and more specific wavefield characteristics than elastic ones (Tsvankin, 1996; Alkhalifah, 1998; Du et al., 2007; Duveneck and Bakker, 2011; Zhan et al., 2012). To describe acoustic wave propagation in anisotropic media, Alkhalifah (1998) adopts pseudo-acoustic approximation to simply the original coupled dispersion relation. Through setting the SVwave velocity along the symmetry axis to zero, one can obtain a pseudo-acoustic wave equation (PWE), which is unphysical but useful for seismic modeling and imaging. Following the idea of the pseudo-acoustic assumption, different variations of PWEs have been exploited for anisotropic modeling and RTM (Zhou et al., 2006; Du et al., 2007; Zhang and Zhang, 2008; Fletcher et al., 2009; Duveneck and Bakker, 2011). However, previous experiences shown that the modeling and imaging results of PWEs may suffer from strong SV-wave artifacts and numercial instability when anisotropy parameters can't meet the pseudo-acoustic assumption, especially for tilted TI (TTI) media with large variations in symmetry dip or azimuth angle (Fletcher et al., 2009). Developing anisotropic pure acoustic wave equations (PAWEs) can

<sup>\*</sup> Corresponding author. Chang'an University, School of Geological Engineering and Geomatics, Department of Geophysics, Xi'an, Shaanxi, 710064, China. E-mail address: xusg2310@chd.edu.cn (S.-G. Xu).

tackle the problem of anisotropic PWEs. Liu et al. (2009) decouple the original P-SV dispersion relation and derive isolated equations for pure-mode P- and SV-waves, respectively. Since then, a series of numercial algorithms have been developed to deal with the decoupled pure-mode disperion relations and wave equations (Chu et al., 2011: Zhan et al., 2012: Sun and Alkhalifah, 2021). These schemes mainly use Taylor expansion (TE) to approximate the original dispersion relation, and then generate the corresponding wave equations. TE methods can only keep high accuracy at small wavenumbers. To improve the accuracy, optimization-based methods and other numerical algorithms get further developments (Alkhalifah, 2013; Fomel et al., 2013; Li and Zhu, 2018; Zhang et al., 2019; Mu et al., 2020; Li et al., 2022). Among them, Li and Zhu (2018) develop an optimal pure acoustic wave dispersion relation and solve the equation by the fast Possion approach. Then, through utilizing different kinds of optimization algorithms to estimate the original pure-mode dispersion relation can effectively balance computational accuracy and efficiency (Zhang et al., 2019; Mu et al., 2020). Following such previous work, we apply a leastsquare (LS) approach for our optimized PAWE modeling and imaging.

On the basis of anisotropy, many researches have been developed in attenuation compensation. Up to now, the constant Q model and generalized standard linear solid (SLS) model are usually adopted to describe the attenuation characteristic of seismic wave. The former uses power exponential functions to depict attenuation and illustrates that the O factor is independent of frequency (Kiartansson, 1979; Carcione et al., 2002; Zhu and Harris, 2014; Zhu et al., 2014: Sun et al., 2015: Chen et al., 2016: Mu et al., 2022). The latter uses a series of SLS elements to approximate the constant Q model in a specific frequency band (Carcione et al., 1988; Blanch et al., 1995; Bai et al., 2014; Blanc et al., 2016; Wang et al., 2019). Compared with the SLS approximation, constant Q model is more accurate, but the solution is more difficult owing to its complexity. To simulate the attenuated mechanisms in anisotropic media, Carcione (1992, 1995) builds the wave equation theory based on the linear viscoelastic anisotropy theory. Zhu and Harris (2014) develop variable spatial fractional Laplacian viscoacoustic wave equation (VAWE) by adopting various approaches for seismic modeling and Q-RTM. Zhu et al. (2014) present a methodology of Q-RTM that can alleviate attenuation and dispersion effects in the migrated images. Bai and Tsvankin (2016) put forward a time-domain FD method for viscoelastic wave modeling in VTI media. Yang and Zhu (2018) derive a time-domain complex-valued wave equation for simulating viscoacoustic wave propagation in frequency-independent Q media. Via transforming fractional time derivatives into fractional Laplacians, Zhu and Bai (2019) implement wavefield modeling in attenuation VTI media. Recently, Hao and Alkhalifah (2019) derive several general expressions of scalar and vector VAWEs in anisotropic media. Xing and Zhu (2019) propose a new spatial independent-order decoupled fractional Laplacian VAWE in anisotropic media. Zhou et al. (2020) decouple the amplitude and phase terms for the VAWE, and develop a Q-compensated RTM frame based on FD algorithm in TTI media. In conclusion, exploiting modified VAWEs for anisotropic pure acoustic wave modeling and RTM is an important research content.

Besides, improving the imaging accuracy is a common goal for seismic exploration. Absorption attenuation, high-speed body shielding, observation system limitation, and so on, may result in insufficient illumination, which can affect the final imaging quality. To improve the resolution for subsalt imaging, many efforts have been proposed, such as, illumination compensation (Liu et al., 2011), walkaway vertical seismic profiling (VSP) RTM (Shi and Wang, 2016), weak signal compensation (Yuan et al., 2016), target-oriented imaging (Chen and Jia, 2014; Song et al., 2021), and

so on.

Our goal is to improve the imaging accuracy for anisotropic *Q*-RTM. Therefore, we share our advancements from the following aspects: first, an optimized pure P-wave equation is established to address the problems of conventional PWEs. Second, a simplified pure-mode VAWE (PVAWE) based on the SLS model is derived. Third, a time-dispersion correlation (TDC) scheme is executed to increase the accuracy. Fourth, we use the target-oriented approach to obtain available reflection and transmission information. Last, the above-mentioned schemes are applied to anisotropic *Q*-RTM based on surface and VSP acquisition geometries. Numerical examples demonstrate the advantages of our proposed schemes.

## 2. A simplified anisotropic pure-mode visco-acoustic wave equation based on optimization strategy

2.1. An optimized pure-mode acoustic wave equation in anisotropic media

The exact P-SV wave dispersion relation in VTI media can be expressed as (Tsvankin, 1996; Alkhalifah, 1998; Pestana et al., 2011)

$$\omega^{2} = \frac{V_{P0}^{2}}{2} \left( (2 - f + 2\varepsilon)k_{x}^{2} + (2 - f)k_{z}^{2} \pm \sqrt{A^{2} - 8(\varepsilon - \delta)fk_{x}^{2}k_{z}^{2}} \right), \tag{1}$$

where  $A=(f+2\varepsilon)k_x^2+fk_z^2$ ,  $\omega$  denotes the angular frequency,  $V_{P0}$  is the P-wave velocity along the symmetry axis,  $\varepsilon$  and  $\delta$  are the Thomsen's anisotropy parameters (Thomsen, 1986).  $k_x$  and  $k_z$  are orthogonal spatial wavenumbers. It is noted that, in Eq. (1), f=1 and the plus sign "+" correspond to P-wave case,  $f=1-\frac{V_{S0}^2}{V_{P0}^2}$  and the minus sign "-" correspond to SV-wave case (Tsvankin, 1996; Alkhalifah, 1998; Pestana et al., 2011). Equation (1) can exactly represent pure-mode dispersion relations in VTI media. However, it is hard to solve this relation by adopting some commonly used numerical methods because of the square root term.

To address the square root in Eq. (1), one first needs to approximate it using several mathematical operations (Zhan et al., 2012; Liu et al., 2009; Chu et al., 2011). By expanding the square root to TE and rearranging it, one can obtain the first-order and second-order approximations as follows (Zhan et al., 2012; Chu et al., 2011):

$$\omega^{2} \approx \frac{V_{P0}^{2}}{2} \left( (2 - f + 2\varepsilon)k_{x}^{2} + (2 - f)k_{z}^{2} \pm \left( A - \frac{4(\varepsilon - \delta)fk_{x}^{2}k_{z}^{2}}{A} \right) \right), \tag{2}$$

$$\omega^{2} \approx \frac{V_{P0}^{2}}{2} \left( (2 - f + 2\varepsilon) k_{x}^{2} + (2 - f) k_{z}^{2} \pm \left( A - \frac{4(\varepsilon - \delta) f k_{x}^{2} k_{z}^{2}}{A} \right) - \frac{8(\varepsilon - \delta)^{2} f^{2} k_{x}^{4} k_{z}^{4}}{A^{3}} \right).$$

$$(3)$$

In comparison with the first-order Eq. (2), the second-order expansion (3) can provide high approximation accuracy, but requires more computational cost. To improve the solving accuracy of pure-mode dispersion relation on the premise of balancing the computational efficiency, we employ a modified strategy to evaluate the square root term in Eq. (1) as follows (Li and Zhu, 2018):

$$\sqrt{A^2 - 8(\varepsilon - \delta)fk_x^2k_z^2} \approx a_1k_x^2 + a_2k_z^2 + \frac{a_3k_x^2k_z^2}{(1 + 2\varepsilon/f)k_x^2 + k_z^2}.$$
 (4)

It can be observed that Eq. (4) is a linear system with respect to right-side expansion coefficients  $a_1$ ,  $a_2$  and  $a_3$ . Based on this feature, via minimizing the difference between left- and right-sides, optimized coefficients can be estimated by computing the following objective function:

$$Error = \iiint \left( \frac{\sqrt{A^2 - 8(\varepsilon - \delta)fk_X^2 k_Z^2} - \sqrt{A^2 - 8(\varepsilon - \delta)fk_X^2 k_Z^2} - \sqrt{a_1 k_X^2 + a_2 k_Z^2 + \frac{a_3 k_X^2 k_Z^2}{(1 + 2\varepsilon/f)k_X^2 + k_Z^2}} \right)^2 dk_X dk_Z.$$
(5)

Substituting Eq. (4) into Eq. (1) and rearranging it, one has

$$\omega^{2} \approx \frac{V_{P0}^{2}}{2} \left( (2 - f + 2\varepsilon \pm a_{1}) k_{x}^{2} + (2 - f \pm a_{2}) k_{z}^{2} \pm \frac{a_{3} k_{x}^{2} k_{z}^{2}}{(1 + 2\varepsilon / f) k_{x}^{2} + k_{z}^{2}} \right), \tag{6}$$

which is the optimized pure-mode dispersion relation.

Equation (6) contains a complicated coupled operator  $\frac{k_x^2k_z^2}{(1+2\varepsilon)f)k_x^2+k_z^2}$ , which is difficult to be solved by several commonly used algorithm for seismic modeling and imaging. To facilitate the calculation, Eq. (6) can be simplified as (Chu et al., 2011; Li and Zhu, 2018)

$$\omega^{2} \approx \frac{V_{P0}^{2}}{2} \left( (2 - f + 2\varepsilon \pm a_{1}) k_{x}^{2} + (2 - f \pm a_{2}) k_{z}^{2} \pm \frac{a_{3} k_{x}^{2} k_{z}^{2}}{k_{y}^{2} + k_{z}^{2}} \right).$$
 (7)

Transforming it to the time-space domain, we obtain

$$\frac{\partial^2 P}{\partial t^2} = V_{P0}^2 \left( b_1 \frac{\partial^2 P}{\partial x^2} + b_2 \frac{\partial^2 P}{\partial z^2} \pm b_3 \frac{\frac{\partial^4}{\partial x^2 \partial z^2}}{\frac{\partial^2}{\partial x^2} + \frac{\partial^2}{\partial z^2}} P \right), \tag{8}$$

where

$$\begin{array}{l} b_1 = (2 - f + 2\varepsilon \pm a_1)/2, \\ b_2 = (2 - f \pm a_2)/2, \\ b_3 = a_3/2. \end{array} \tag{9}$$

To solve Eq. (8), we introduce an auxiliary wavefield U and separate it into two parts as follows (Chu et al., 2011; Li and Zhu, 2018)

$$\frac{\partial^2 P}{\partial t^2} = V_{P0}^2 \left( b_1 \frac{\partial^2 P}{\partial x^2} + b_2 \frac{\partial^2 P}{\partial z^2} \pm b_3 \frac{\partial^4 U}{\partial x^2 \partial z^2} \right), \tag{10}$$

$$\frac{\partial^2 U}{\partial x^2} + \frac{\partial^2 U}{\partial z^2} = \nabla^2 U = P. \tag{11}$$

Equations (10) and (11) represent the optimized pure-mode wave equations. Among them, Eq. (10) is an explicit form and can be computed by regular-grid FD, Eq. (11) is an implicit one and can be solved by using Possion method (Li and Zhu, 2018), in which we briefly describe the implementation procedure in Appendix A.

If we adopt rotated wavenumbers  $\hat{k}_X$  and  $\hat{k}_Z$  to replace orthogonal wavenumbers  $k_X$  and  $k_Z$  in Eqs. (1)–(7), and employ rotated derivatives  $\frac{\partial^2}{\partial \hat{x}^2}$  and  $\frac{\partial^2}{\partial \hat{z}^2}$  to replace orthogonal derivatives  $\frac{\partial^2}{\partial x^2}$  and  $\frac{\partial^2}{\partial z^2}$  in Eqs. (8)-(10), one can obtain pure-mode dispersion relation and wave equation in TTI media. The wavenumbers and derivatives in orthogonal and rotated coordinate systems have the following

relations, respectively,

$$\hat{k}_X = k_X \cos \theta - k_Z \sin \theta, \ \hat{k}_Z = k_X \sin \theta + k_Z \cos \theta, \tag{12}$$

and

$$\frac{\partial^{2}}{\partial \dot{x}^{2}} = \cos^{2}\theta \frac{\partial^{2}}{\partial x^{2}} + \sin^{2}\theta \frac{\partial^{2}}{\partial z^{2}} - \sin^{2}\theta \frac{\partial^{2}}{\partial x \partial z}, 
\frac{\partial^{2}}{\partial \dot{z}^{2}} = \sin^{2}\theta \frac{\partial^{2}}{\partial x^{2}} + \cos^{2}\theta \frac{\partial^{2}}{\partial z^{2}} + \sin^{2}\theta \frac{\partial^{2}}{\partial x \partial z},$$
(13)

where  $\boldsymbol{\theta}$  denotes the dip angle of the symmetry axis in TTI media.

It should be emphasized that, in the following seismic wave modeling and imaging, we are mainly interested in the P-wave component and will focus on f = 1 and "+" in Eqs. (2)-(10).

To examine the accuracy, Fig. 1 displays several snapshots for a three-layered model. The model size is 3000 m  $\times$  3000 m, the depths of the second and third layers are 1050 m and 1800 m, respectively. Other parameters are depicted in Fig. 1(a). For comparison, we adopt PWEs with zero and nonzero S-wave velocities to produce pseudo-acoustic wavefields (Du et al., 2007; Fletcher et al., 2009). From these figures, one can observe that the wavefield computed by PWE with zero S-wave velocity suffers from instability. The pseudo-acoustic wavefield using nonzero S-wave velocity contains strong SV-wave artifacts. The slice generated by optimized pure P-wave equation is free from SV-waves while preserving the P-wave event better.

### 2.2. Extending pure-mode acoustic wave equation to attenuation media

Here, we first review a kind of simplified VAWE in isotropic media. Based on the SLS model (Carcione et al., 1988; Blanch et al., 1995; Bai et al., 2014; Blanc et al., 2016), Wang et al. (2019) propose a simplified VAWE, which both considers amplitude attenuation and phase distortion, as follows:

$$\frac{\partial^2 P}{\partial t^2} = \underbrace{v^2 \Delta P}_{part 1} - \underbrace{\frac{part 2}{7v \sqrt{-\Delta}} \frac{\partial}{\partial t} P}_{part 2} - \underbrace{\frac{part 3}{\sqrt{Q^2 + 1} - 1} v^2 \Delta P}_{q^2}, \tag{14}$$

where, v is velocity in isotropic media,  $\Delta = \frac{\partial^2}{\partial x^2} + \frac{\partial^2}{\partial z^2}$  is Laplacian operator, Q is quality factor,  $\tau$  is relaxation variable and is function of the quality factor Q as follows:

$$\tau = \frac{\tau_{\varepsilon}}{\tau_{\delta}} - 1,$$

$$\tau_{\varepsilon} = \frac{\sqrt{Q^2 + 1} + 1}{\omega_0 Q},$$

$$\tau_{\delta} = \frac{\sqrt{Q^2 + 1} - 1}{\omega_0 Q},$$
(15)

where  $\omega_0$  is the reference angular frequency. As described in the right side of Eq. (14), the first term (part 1) is the original acoustic wave equation, the second term (part 2) depicts the amplitude attenuation, and the third term (part 3) depicts the phase distortion, respectively. We can combine FD and pseudo-spectral method (PSM) to calculate it (Wang et al., 2019). When Q is infinite, Eq. (14) degenerates to the isotropic acoustic wave equation.

For anisotropic media, there are less studies on the corresponding VAWEs, especially for pure acoustic media. Therefore, we

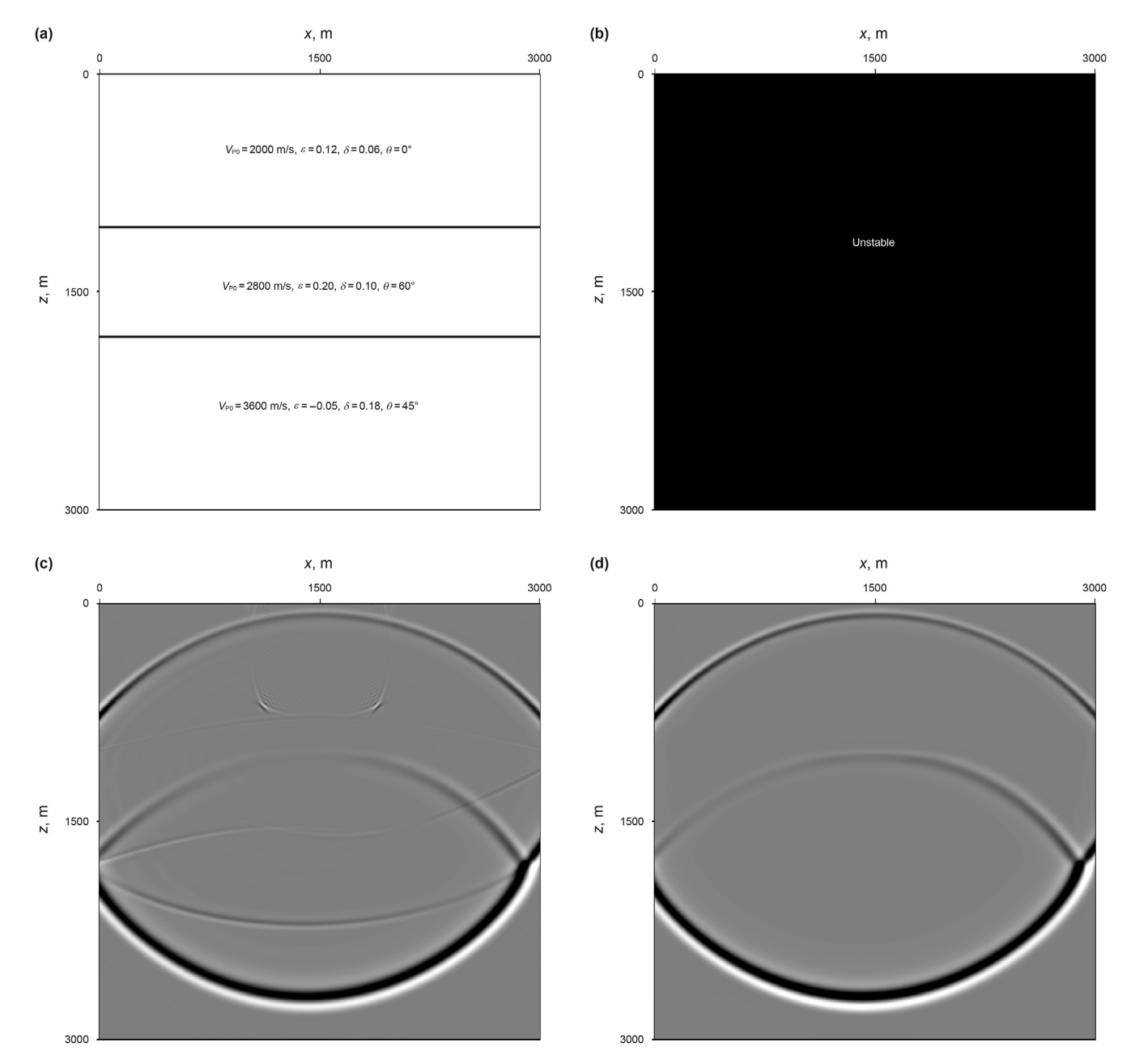


Fig. 1. Wavefield slices in (a) a three-layered anisotropic model calculated by (b) PWE with zero S-wave velocity, (c) PWE with nonzero S-wave velocity and (d) the optimized pure P-wave equation, respectively.

develop a simplified PVAWE by combining the above-mentioned isotropic SLS-based VAWE and optimized PAWE. We start from PAWE (10) and rewrite it as a unified form as follows:

$$\frac{\partial^2 P}{\partial t^2} = V_{P0}^2 \mathbf{H} P,\tag{16}$$

in which, the operator H can be expressed as

$$\boldsymbol{H}P = b_1 \frac{\partial^2 P}{\partial x^2} + b_2 \frac{\partial^2 P}{\partial z^2} + b_3 \frac{\partial^4 U}{\partial x^2 \partial z^2}.$$
 (17)

It can be observed that, the operator  $\Delta$  in Eq. (14) and the operator  $\boldsymbol{H}$  in Eq. (17) both consist of different partial derivatives, which are related to the wavefield. Thus, if one adopts operator  $\boldsymbol{H}$  to replace  $\Delta$ , we can obtain a simplified PVAWE in anisotropic media

as follows:

$$\frac{\partial^2 P}{\partial t^2} = V_{P0}^2 \boldsymbol{H} P - \frac{\tau V_{P0}}{2} \sqrt{-\Delta} \ \frac{\partial}{\partial t} P - \frac{\sqrt{Q^2 + 1} - 1}{Q^2} V_{P0}^2 \boldsymbol{H} P, \tag{18}$$

the solution of the term HP has illustrated in the previous section. The term  $\sqrt{-\Delta} \frac{\partial}{\partial t} P$  can be computed by the PSM as follows:

$$\sqrt{-\Delta} \frac{\partial}{\partial t} P = \mathbf{F}^{-1} \left[ |\mathbf{k}| \mathbf{F} \left( \frac{P_{0,0}^0 - P_{0,0}^{-1}}{\Delta t} \right) \right], \tag{19}$$

where  $\mathbf{k}$  denotes the wavenumber vector,  $\mathbf{F}$  and  $\mathbf{F}^{-1}$  are Fourier forward and inverse transforms.

Compared with the anisotropic acoustic Eq. (16), Eq. (18)

includes two additional terms that represent the amplitude attenuation and phase distortion. If the phase distortion is disappeared, Eq. (18) becomes

$$\frac{\partial^2 P}{\partial t^2} = V_{P0}^2 \mathbf{H} P - \frac{\tau V_{P0}}{2} \sqrt{-\Delta} \frac{\partial}{\partial t} P. \tag{20}$$

Similarly, when the amplitude attenuation is ignored, Eq. (18) is reduced to

$$\frac{\partial^2 P}{\partial t^2} = V_{P0}^2 \mathbf{H} P - \frac{\sqrt{Q^2 + 1} - 1}{Q^2} V_{P0}^2 \mathbf{H} P. \tag{21}$$

Using a homogeneous anisotropic model to test the equations introduced above, the model parameters are  $V_{P0} = 3000$  m/s,  $\varepsilon = 0.20$ ,  $\delta = 0.05$ ,  $\theta = 45^{\circ}$ , Q = 20, respectively. In Fig. 2(a), we display partial snapshots from the PAWE (16), the amplitude attenuation Eq.

(20), the phase distortion equation (21), and the PVAWE (18). Compared with the PAWE, the results from Eqs. (20) and (21) can only result in amplitude attenuation or phase shift. In contrast, the PVAWE takes both the amplitude attenuation and phase distortion into consideration, and describes the attenuation feature better for anisotropic media. Besides, several waveform curves are displayed in Fig. 2(b), the same conclusion can be obtained.

#### 3. Time-dispersion correlation strategy

A second-order FD is usually applied to estimate second-order time derivative of the anisotropic wave equation, such as  $\frac{\partial^2 P}{\partial t^2} \approx \frac{P_{j,l}^{o+1} - 2P_{j,l}^o + P_{j,l}^{o-1}}{\Delta t^2}$ , where  $\Delta t$  is the time sampling interval. The second-order accurate FD discretization may give rise to accumulated temporal error during wavefield extrapolation. Koene et al. (2018) demonstrate that this kind of the time dispersion error

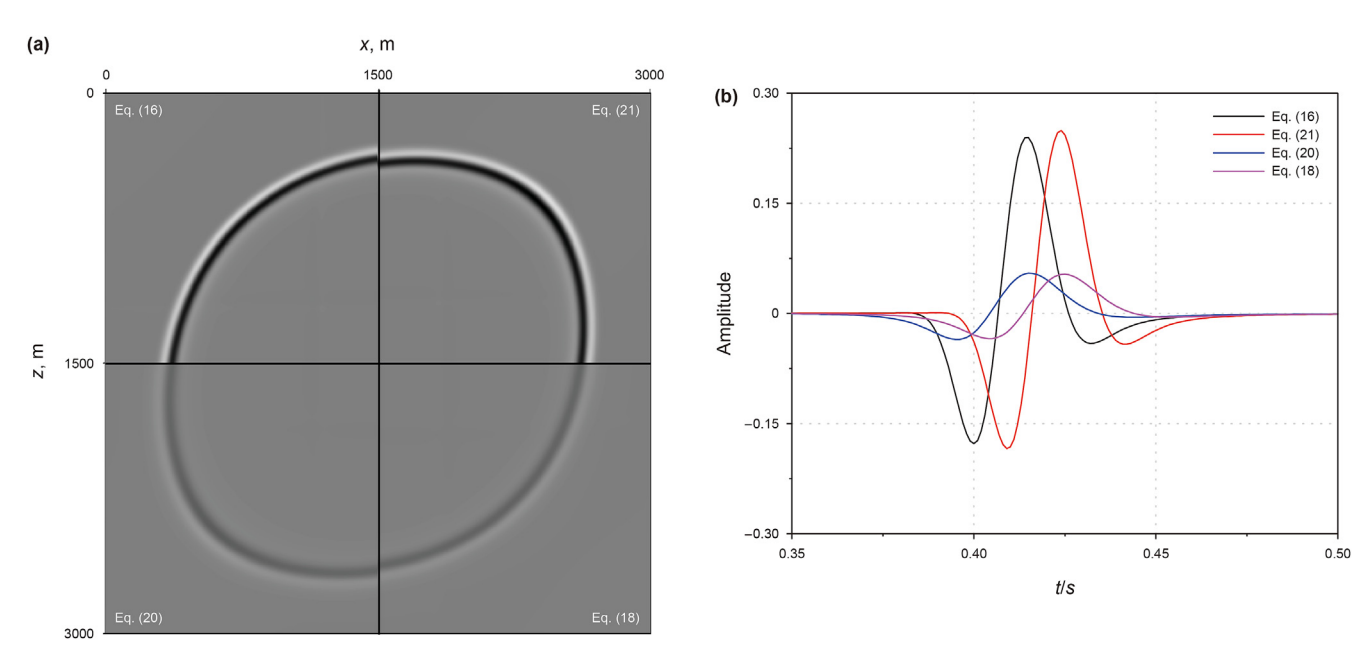
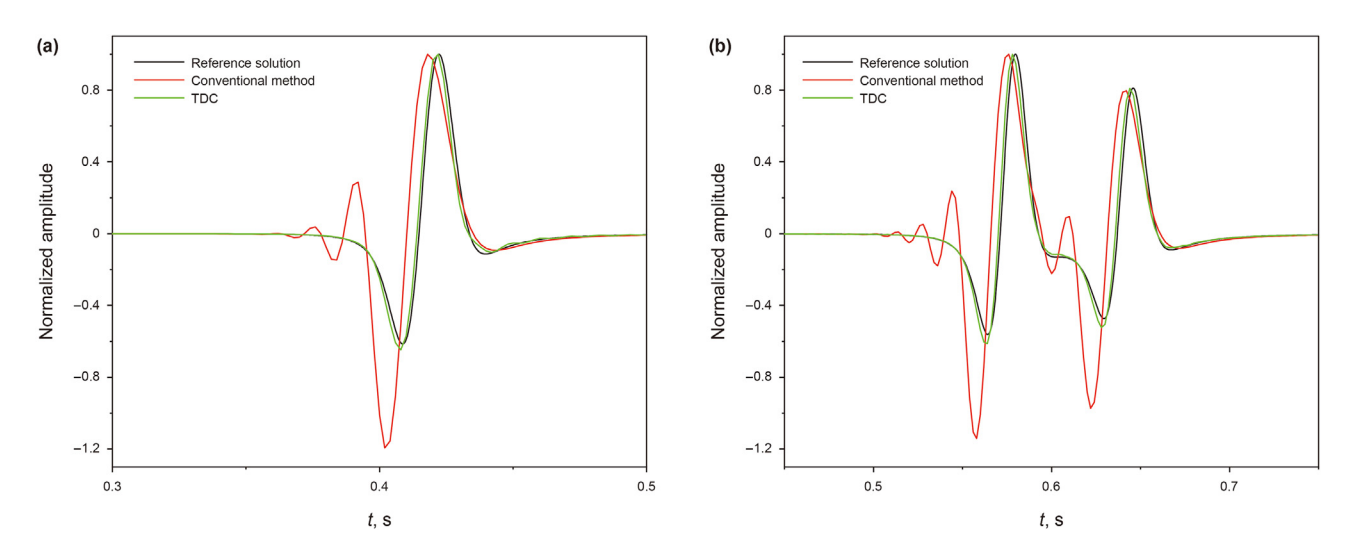


Fig. 2. Simulated results computed by different equations for a homogeneous anisotropic model. (a) Partial snapshots, (b) waveform curves.



**Fig. 3.** Waveform curves in a homogeneous anisotropic model computed using the reference solution, conventional method, and time-dispersion correction (TDC), respectively. Note that (a) is extracted from surface seismic record and (b) is extracted from VSP seismic record, respectively. The reference solution is produced by the conventional method with a long FD operator and a fine time step.

accelerates the input signal as a function of frequency and time step only, and thus is independent of the medium type, propagation path and spatial simulation error. Given these facts, they estimated the time dispersion error by the forward time dispersion transform (FTDT) and restrained the time dispersion from seismic records by the inverse time dispersion transform (ITDT). It has been reported that the related results hold for any time-invariant medium, spatial simulation error, and is suitable for any forms of the second-order wave equations (Koene et al., 2018). Their proposed schemes can generate high numerical precision in wavefield simulation and imaging. Here, to suppress time dispersion errors from anisotropic seismic traces, we directly extend this effective scheme to our anisotropic attenuation wavefield simulation and RTM workflow, and refer to the following processes (Koene et al., 2018):

(1) For an input seismic wavelet, we pre-process it with FTDT.

- (2) Based on step (1), perform the standard pure-mode seismic wavefield extrapolation and generate desired seismic records.
- (3) Apply ITDT to recorded seismograms from step (2), and produce the time dispersion-free seismograms on both surface and VSP observation systems.

Using a homogeneous anisotropic model to test the above-mentioned scheme. The time step is 0.002 s. The related parameters are  $V_{P0}=2400$  m/s,  $\varepsilon=0.2$ ,  $\delta=0.1$ ,  $\theta=45^{\circ}$ , and Q=30, respectively. A Ricker wavelet with the main frequency of 40 Hz is used to produce the vibration. Fig. 3 shows several waveform curves extracted from surface and VSP seismic records computed by different methods. From this figure, one observes that the waveforms of the conventional method have strong numerical error. By contrast, the time-dispersion correlation can significantly

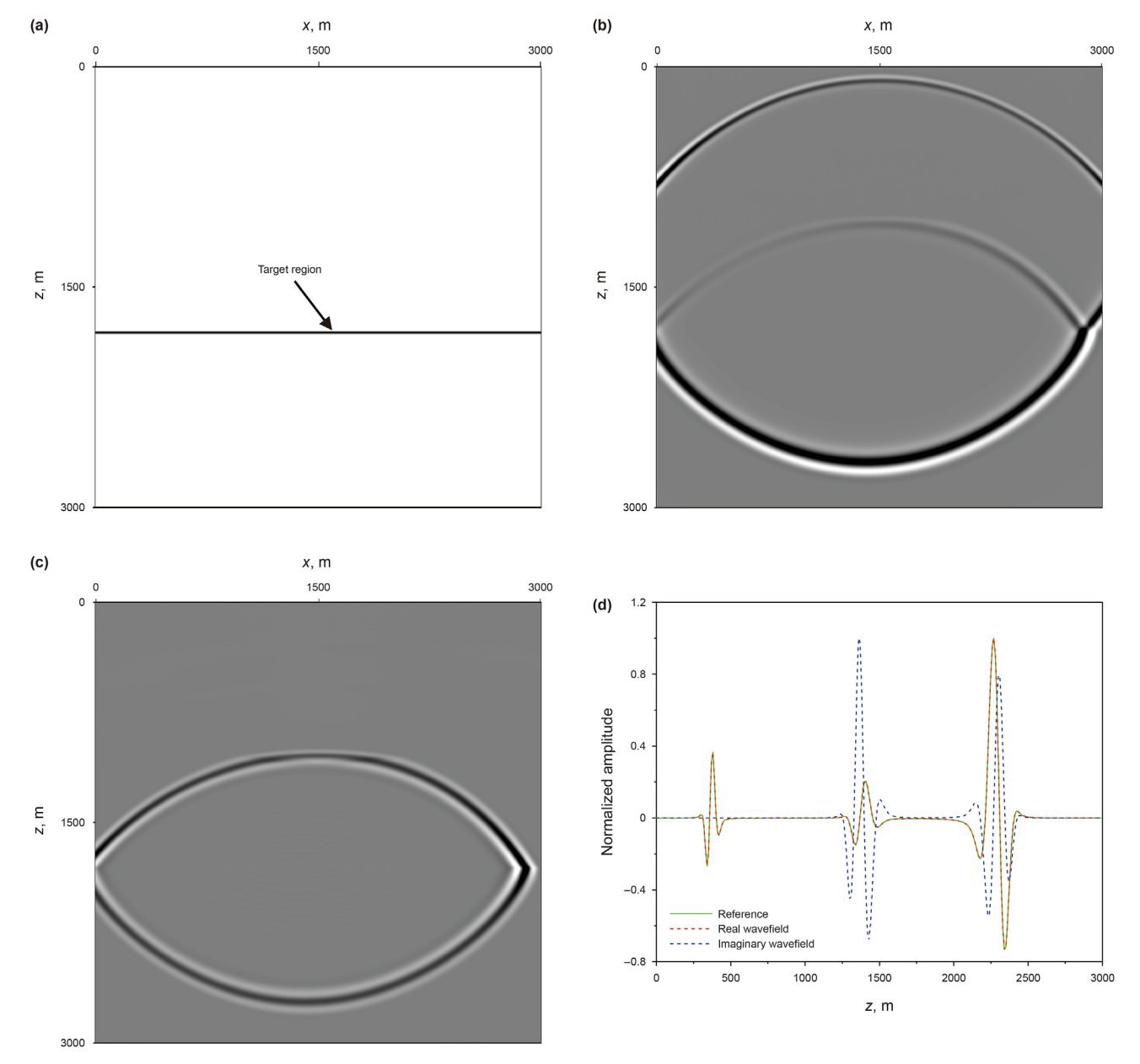


Fig. 4. Wavefield modeling results in anisotropic three-layered complex model. (a) The imaginary part of the velocity model, the depth of the target region is 1800 m and  $\tilde{V} = \overline{V} \times 10^{-6}$ . The real part is described in Fig. 3(a). (b) The real wavefield slice, (c) the imaginary wavefield slice, and (d) several waveform curves extracted from real and imaginary wavefields.

enhance the simulation accuracy, because the waveform curves match the reference curves much better.

#### 4. Target-oriented PVAWE modeling and imaging

#### 4.1. Target-oriented PVAWE modeling

In this section, we establish a target-oriented modeling scheme to extract more available wavefield information related to the target structure in anisotropic attenuation media (Chen and Jia, 2014).

We first adopt a uniform expression to rewrite optimized PVAWE (18) as follows:

$$\frac{\partial^2 P}{\partial t^2} = V^2 \Theta P,\tag{22}$$

where 
$$V=V_{P0},~\Theta P=\left(\mathbf{H}P-\frac{\tau}{2V_{P0}}\sqrt{-\Delta}~\frac{\partial}{\partial t}P-\frac{\sqrt{Q^2+1}-1}{Q^2}\mathbf{H}P\right)$$
, the

solution of auxiliary wavefield U has been illustrated earlier. To construct a wavefield that only includes reflection and transmission information relevant to the target structure, we extend the target-oriented wavefield extrapolation algorithm to our anisotropic media (Chen and Jia, 2014; Song et al., 2021).

Using a second-order FD to estimate temporal derivative, the extrapolated scheme for Eq. (22) can be simplified as

$$P_{i,l}^{o+1} = V^2 P^o + 2P_{i,l}^o - P_{i,l}^{o-1}, (23)$$

where  $P^0 = (\Delta t/h)^2 \Lambda P^0$ , operational character  $\Lambda P^0$  denotes the discretization scheme of differential operator  $\Theta P$  in Eq. (22).

To conduct the target-oriented algorithm, we extend wavefield variables to the complex domain as follows (Chen and Jia, 2014):

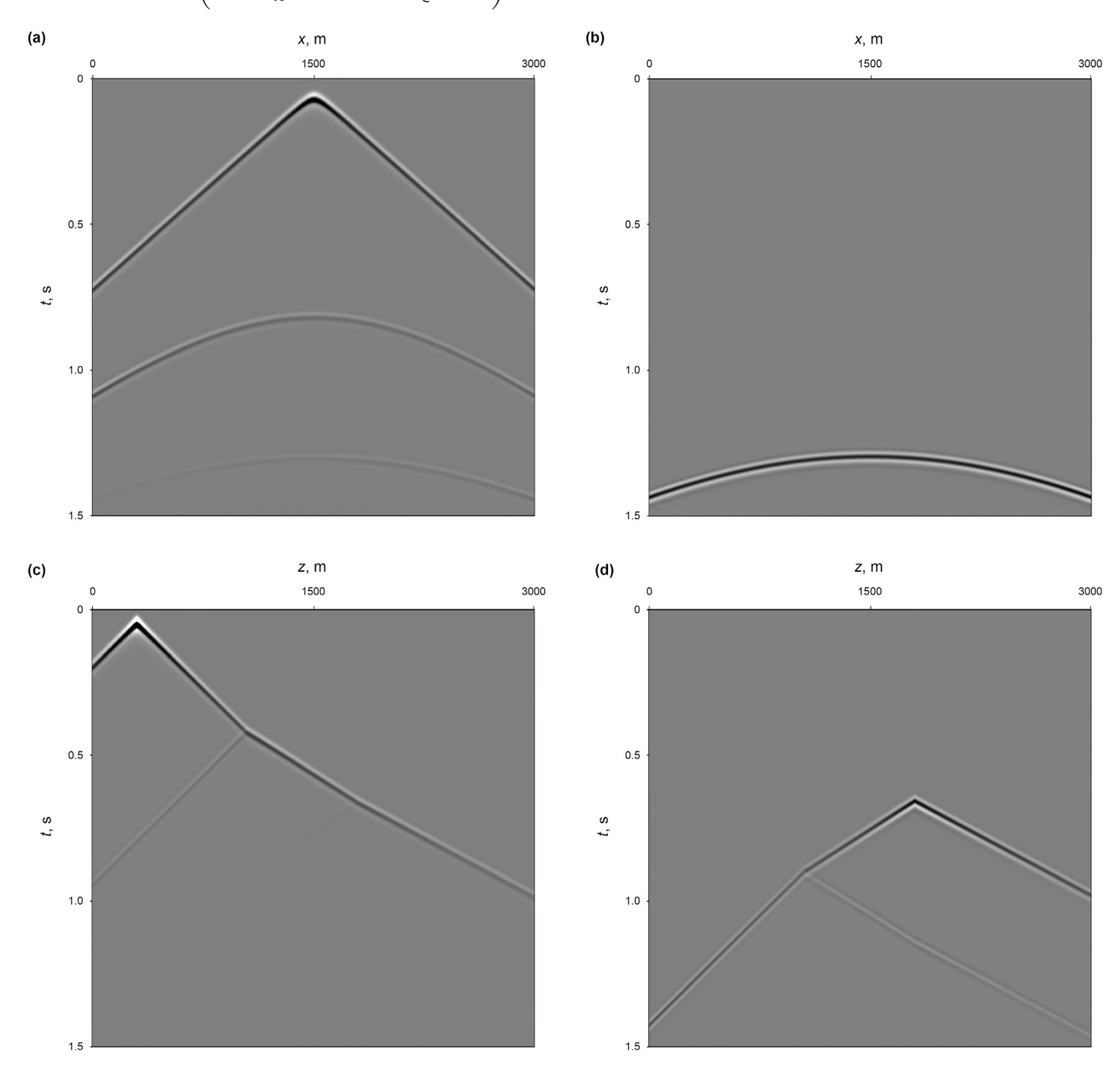
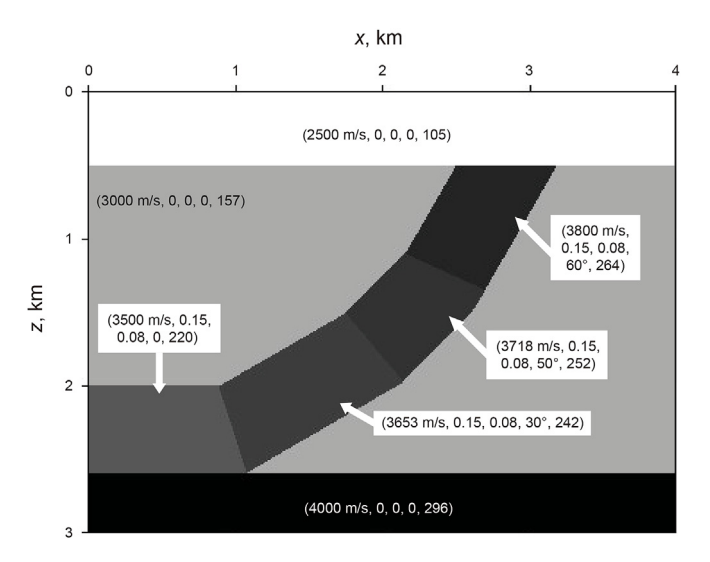


Fig. 5. Seismic records in anisotropic three-layered complex model. (a, b) Modeling results on surface observation system. (c, d) Modeling results on VSP observation system. (a, c) are based on real velocity field, (b, d) are based on imaginary velocity field.



**Fig. 6.** A modified anisotropic fault model. The related parameters  $(V_{p0},\ \varepsilon,\ \delta,\ \theta,\ Q)$  are depicted in the figure.

$$P_{i,l}^0 = \overline{P}_{i,l}^0 + i\tilde{P}_{i,l}^0, \tag{24}$$

$$P^{o} = \overline{P}^{o} + i\tilde{P}^{o}, \tag{25}$$

$$V_{i,l} = \overline{V}_{i,l} + i\tilde{V}_{i,l},\tag{26}$$

where i denotes the imaginary unit, the symbol "–" of all variables is the real part, and the symbol "~" is the imaginary part, respectively. Substituting Eqs. (24)–(26) into (23), and rearranging the iteration scheme in complex domain yield

$$\left(\overline{P}_{j,l}^{o+1} + i\widetilde{P}_{j,l}^{o+1}\right) = \left(\overline{V}_{j,l} + i\widetilde{V}_{j,l}\right)^{2} \left(\overline{P}^{o} + i\widetilde{P}^{o}\right) + 2\left(\overline{P}_{j,l}^{o} + i\widetilde{P}_{j,l}^{o}\right) - \left(\overline{P}_{j,l}^{o-1} + i\widetilde{P}_{j,l}^{o-1}\right).$$
(27)

Based on Eq. (27), the iteration schemes in the real and imaginary domains can be respectively expressed as

$$\overline{P}_{j,l}^{o+1} = \overline{V}_{j,l}^{2} \overline{P}^{o} + 2 \overline{P}_{j,l}^{o} - \overline{P}_{j,l}^{o-1} - 2 \overline{V}_{j,l} \tilde{V}_{j,l} \tilde{P}^{o} - \tilde{V}_{j,l}^{2} \overline{P}^{o},$$
 (28)

$$\tilde{P}_{j,l}^{o+1} = \overline{V}_{j,l}^{2} \tilde{P}^{o} + 2 \tilde{P}_{j,l}^{o} - \tilde{P}_{j,l}^{o-1} + 2 \overline{V}_{j,l} \tilde{V}_{j,l} \overline{P}^{o} - \tilde{V}_{j,l}^{2} \tilde{P}^{o}.$$
 (29)

The target-oriented technique is carried out by assigning an infinitesimal value to the imaginary part of the velocity; i.e., (Chen and Jia, 2014):

$$\overline{V}_{j,l} = V_{j,l}, \tilde{V}_{j,l} \begin{cases} \neq 0, & \text{within target region} \\ = 0, & \text{within other region} \end{cases}$$
 (30)

In practical terms,  $\tilde{V}_{j,l}$  is of the  $10^{-6}$  order of magnitude (Chen and Jia, 2014). For our anisotropic attenuation modeling and imaging, it should be emphasized that the velocity and wavefield components are complex values, whereas the anisotropy parameters, dip angle and Q factor all are real values.

#### 4.2. Target-oriented Q-RTM

The target-oriented approach can be extended to anisotropic RTM to produce an image of the target structure. The implementation is divided into as (Chen and Jia, 2014):

- (1) Extrapolating the forward-propagating real wavefield  $S_r(x, z, t)$  and imaginary wavefield  $S_i(x, z, t)$  in the complex domain.
- (2) Extrapolating the backward-propagating wavefield R(x, z, t) only in the real domain.
- (3) Applying the modified imaging conditions to generate two kinds of the final profiles as follows:

$$I_r(x,z) = \int_0^T S_r(x,z,t) R(x,z,T-t) dt,$$
 (31)

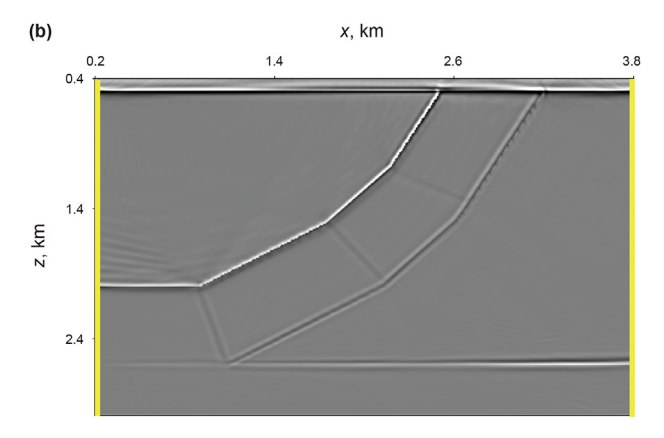


**Fig. 7.** Imaging results for the modified anisotropic fault model on (a) surface observation system, (b) VSP observation system, respectively. The receivers positions of VSP observation system are x = 200 m and x = 3800 m, respectively, as denoted by yellow vertical lines.

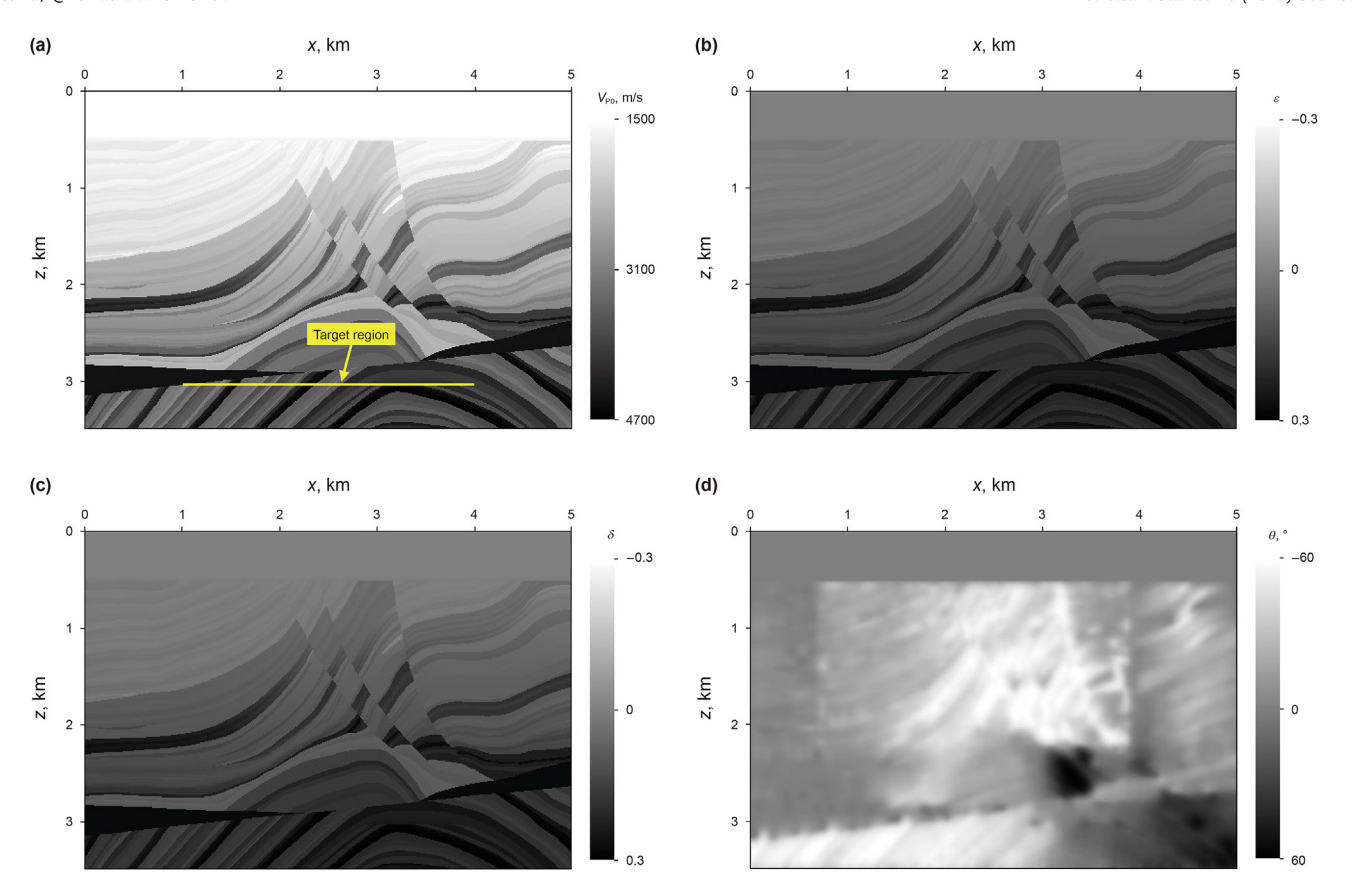


Fig. 8. The modified anisotropic Marmousi model. (a)  $V_{P0}$ , (b)  $\varepsilon$ , (c)  $\delta$ , (d)  $\theta$ . Note that (a) is real velocity field, the imaginary velocity field is denoted by the yellow line in (a) and has 1000 m  $\leq x \leq 4000$  m and z = 3080 m. The imaginary velocity  $\bar{V}$  is  $V_{P0} \times 10^{-6}$  for target region and 0 for non-target region, respectively.

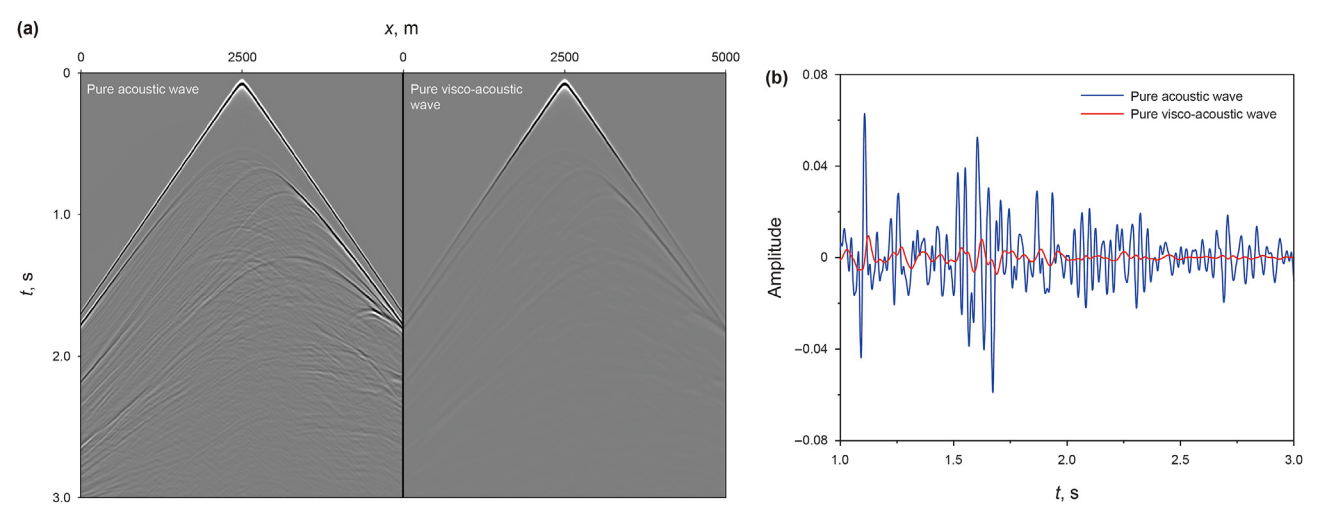


Fig. 9. Simulated results computed by anisotropic pure acoustic wave and pure visco-acoustic wave equations for the modified Marmousi anisotropic model. (a) Seismic records, (b) waveform curves.

$$I_{i}(x,z) = \int_{0}^{T} S_{i}(x,z,t)R(x,z,T-t)dt,$$
(32)

where, the term  $I_r(x, z)$  is the *real imaging result*, which is exactly the same as the result of the standard RTM, and  $I_i(x, z)$  is the *imaginary* 

*imaging result* that can be regarded as the image of the target structure, which can be considered supplementary to the traditional RTM.

To test the target-oriented wavefield modeling algorithm, we design a three-layered complex velocity model, the real part is shown in Fig. 1(a) and the Q factors of three layers are 30, 50 and 80, respectively. The imaginary part is described in Fig. 4(a). Fig. 4(b)

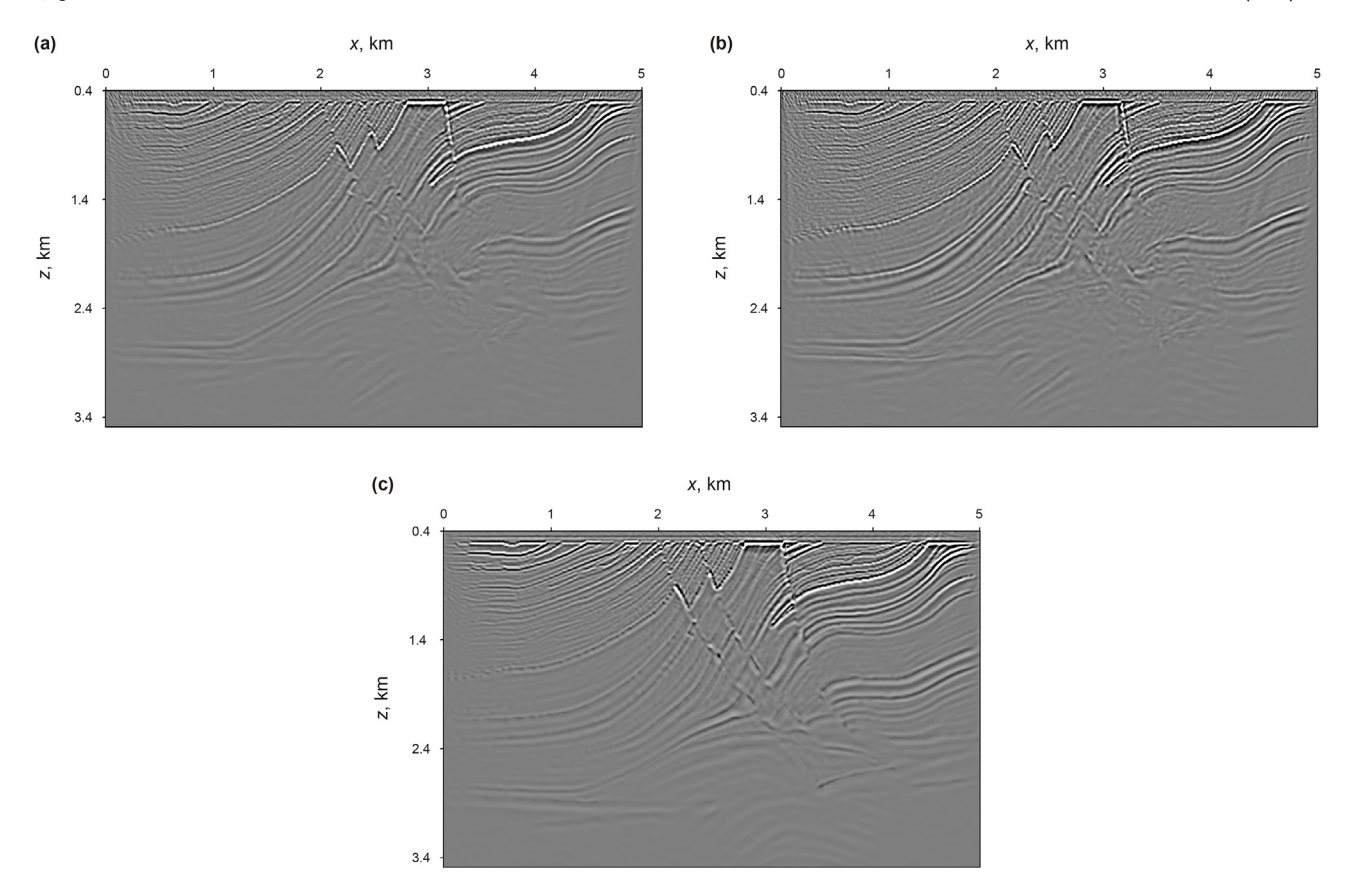


**Fig. 10.** Surface imaging results for the modified anisotropic Marmousi model generated by (a) the isotropic acoustic wave equation, (b) the isotropic visco-acoustic wave equation, (c) the anisotropic pure-mode acoustic wave equation, respectively.

and (c) show two kinds of wavefield snapshots for this complex model. Comparing the slices of the real and imaginary wavefields, we observe that the imaginary wavefield only contains the transmission and reflection informations relevant to the target region, that is the second reflector. Note that the reference curve is computed by PVAWE with the original velocity model. Fig. 4(d) displays several normalized waveform curves of the real and imaginary wavefields. The waveform of the real wavefield is closed to the reference waveform on account of the imaginary velocity approaching an infinitesimal value. Compared to the reference, the imaginary wavefield associated with the first layer is restrained, but the transmission and reflection characteristics related to the target structure come to the front. Fig. 5 exhibits several seismic records on surface and VSP observation systems, the same conclusions can be obtained.

Considering that the amplitude is attenuated in PVAWE (18), the amplitude should be compensated in the forward- and backward-propagating during Q-RTM. To ensure the stability of wavefield propagation, we add a regularization operator to PVAWE (18). This operator is actually a low-pass filter that is a function of the wavefield velocity and Q factor. Following the previous research (Wang et al., 2019), the PVAWEs for the forward-propagating wavefield  $P_f$  and backward-propagating wavefield  $P_b$  are modified as

$$\frac{\partial^{2} P_{f}}{\partial t^{2}} = \varphi_{1} \mathbf{H} P_{f} + \varphi_{2} \sqrt{-\Delta} \frac{\partial}{\partial t} P_{f} + \varphi_{3} \mathbf{H} P_{f} + \varphi_{4} \frac{\partial}{\partial t} \mathbf{H} P_{f}, \tag{33}$$

and

$$\frac{\partial^{2} P_{b}}{\partial t^{2}} = \varphi_{1} \mathbf{H} P_{b} + \varphi_{2} \sqrt{-\Delta} \frac{\partial}{\partial t} P_{b} + \varphi_{3} \mathbf{H} P_{b} + \varphi_{4} \frac{\partial}{\partial t} \mathbf{H} P_{b}, \tag{34}$$

where,

$$\varphi_{1} = V_{P0}^{2}, 
\varphi_{2} = \frac{\tau V_{P0}}{2}, 
\varphi_{3} = \frac{1 - \sqrt{Q^{2} + 1}}{Q^{2}} V_{P0}^{2}, 
\varphi_{4} = \frac{\tau \alpha}{2} V_{P0}^{2}.$$
(35)

the fourth term in the right-side of Eqs. (33) and (34) is regularization item, which is mainly adopted to deal with the instability during wavefield compensation. The compensated effect depends on the choice of the parameter  $\alpha$ . With the decrease of  $\alpha$ , the effect becomes better, but the stability becomes poor.

#### 5. Numerical examples

First, a modified anisotropic fault model is used to examine the proposed scheme. The model size is 4000 m  $\times$  3000 m, and the model parameters are displayed in Fig. 6. Fig. 7 provides two imaging profiles produced by anisotropic pure-mode visco-acoustic wave. It can be observed that, the imaging method on VSP observation system can produce higher accuracy than surface RTM for inclined structures. Moreover, the imaging resolution can be

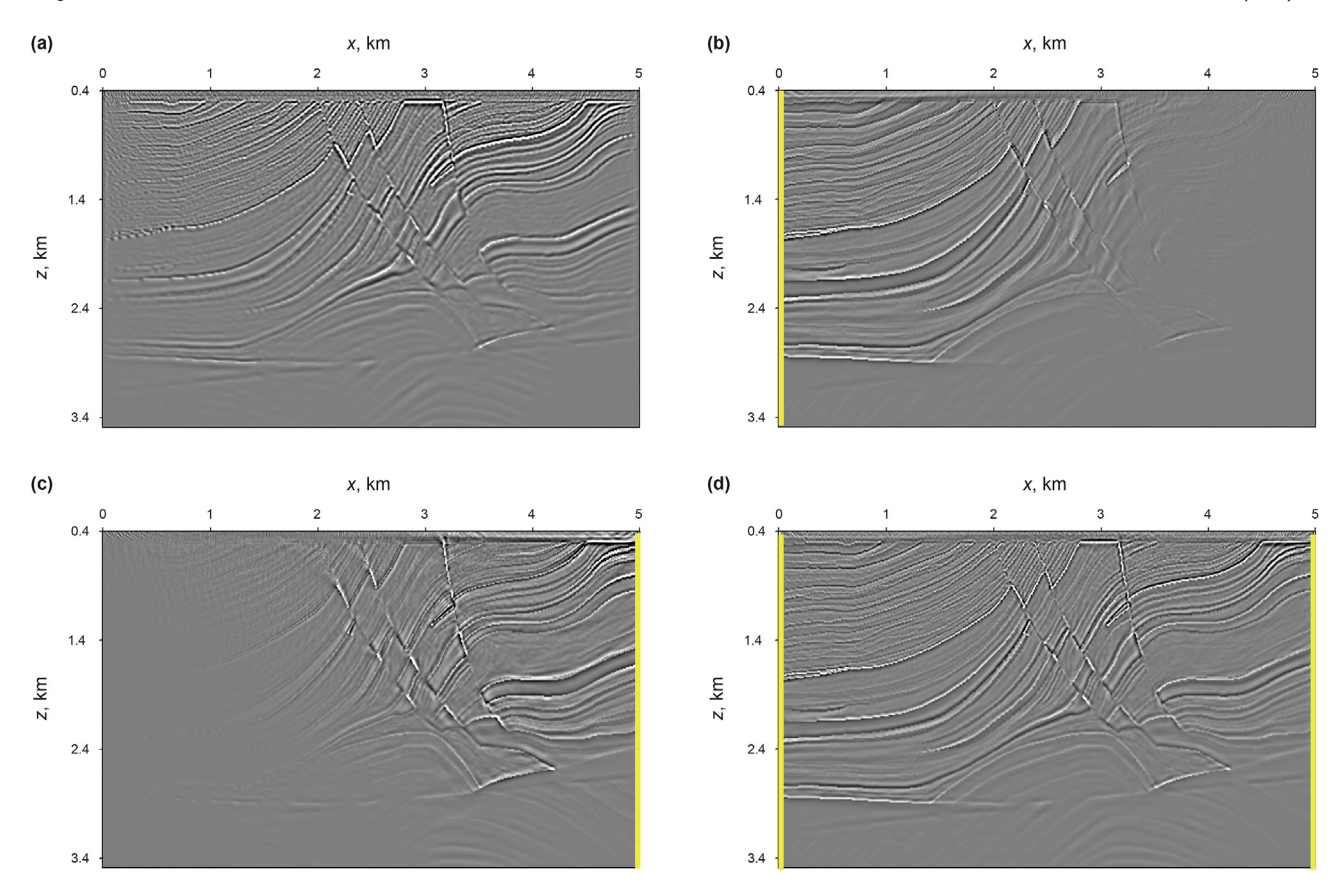


**Fig. 11.** Real imaging results for the modified anisotropic Marmousi model generated by the optimized pure-mode visco-acoustic wave equation. (a) Surface image, (b, c) VSP images, (d) surface + VSP images. The receivers depth of surface observation system is z = 100 m. The receivers positions of VSP observation system are x = 10 m and x = 4990 m, respectively, as denoted by yellow vertical lines.

effectively improved by combining surface and VSP RTM schemes.

Then, we adopt the modified anisotropic Marmousi model, as depicted in Fig. 8, to test the above-mentioned methods. The model size is 5000 m  $\times$  3500 m. The source signal is represented by a Ricker wavelet with the peak frequency of 24 Hz. The Q model is generated by the empirical formula of  $Q=3.516\times V_{P0}^{2.2}\times 10^{-6}$ . Fig. 9 displays several simulated results. It can be seen that, compared with the PAWE, the proposed PVAWE takes amplitude attenuation and phase distortion into consideration simultaneously, and can depict the attenuation characteristics better for complicated anisotropic model. Figs. 10–12 illustrate several imaging profiles computed by different schemes. Note that we have applied Laplace filtering to all slices. From these figures, one can conclude that,

- (1) For the seismic records produced by the PVAWE, the imaging results of the isotropic acoustic wave, isotropic VAWE and anisotropic PAWE all lead to malposed imaging profiles and low resolution of the geologic targets, as displayed in Fig. 10.
- (2) In comparison with conventional imaging schemes, our developed PVAWE-based Q-compensated RTM can greatly enhance the imaging accuracy and resolution. The imaging method on VSP observation system can generate higher resolution near the well than surface RTM. Through

- incorporating VSP image and surface image, one can obtain satisfactory imaging result, as shown in Fig. 11.
- (3) Compared with real images, the imaginary ones can provide available structure informations near the target region. Therefore, these two kinds of imaging methods can complement each other, and generate high accuracy RTM results for complicated anisotropic media, as depicted in Fig. 12.

#### 6. Conclusions

We have developed several technical improvements for anisotropic Q-RTM. A least-square-based pure P-wave equation is derived to address the traditional pseudo-shear wave artifacts and propagation instability. Then, a simplified pure visco-acoustic wave equation is established by combining pure P-wave equation and standard linear solid-based isotropic visco-acoustic wave equation. To suppress numercial dispersion errors for attenuated wavefield extrapolation and imaging, a time-dispersion correction approach is adopted. To generate high quality imaging for complicated target structures, a target-oriented anisotropic modeling and imaging, which can extract effective reflection and transmission informations near the target regions, is exploited. We jointly apply the above-mentioned schemes to anisotropic surface and VSP Q-

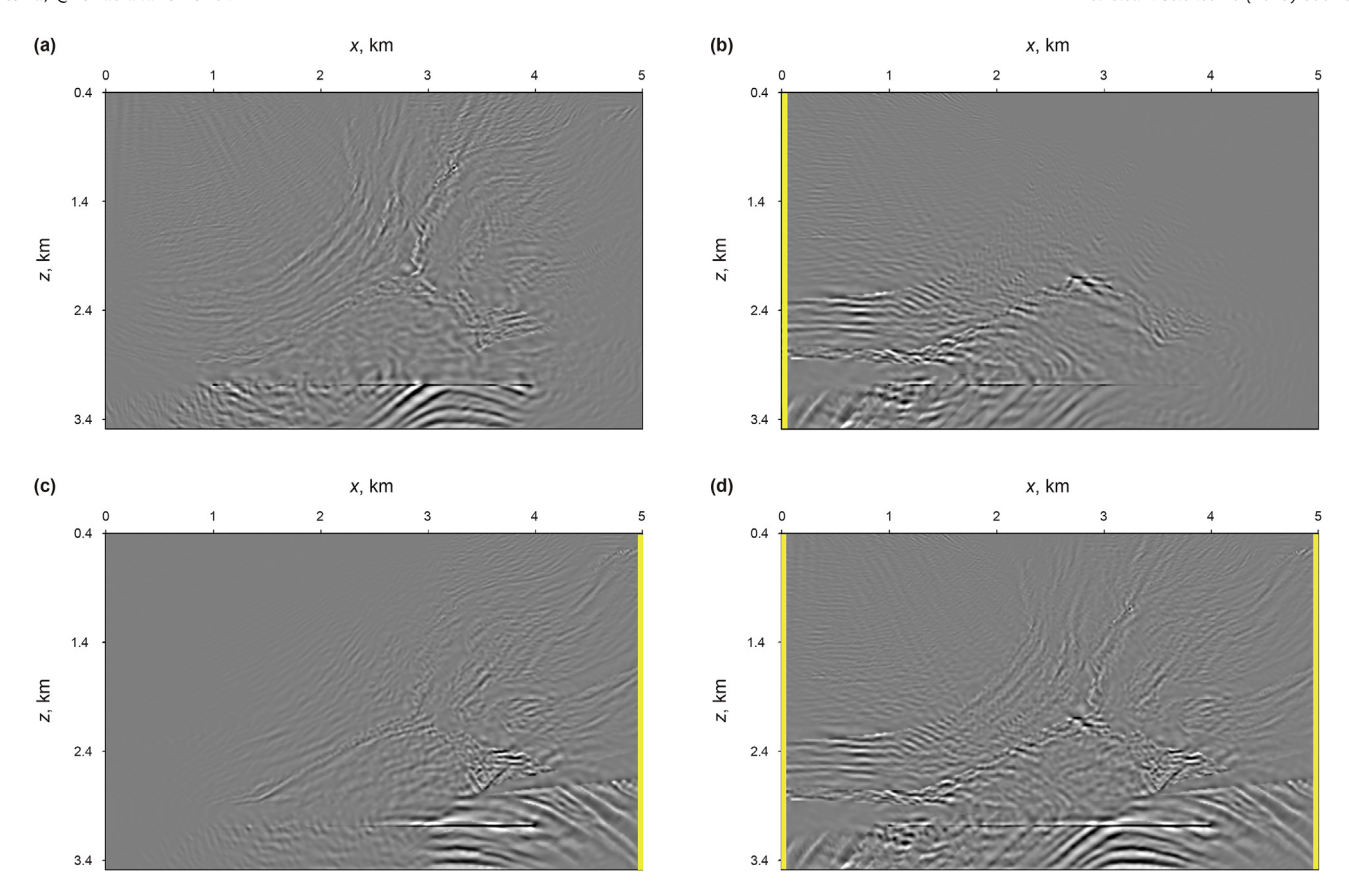


**Fig. 12.** Imaginary imaging results for the modified anisotropic Marmousi model generated by the optimized pure-mode visco-acoustic wave equation. (a) Surface image, (b, c) VSP images, (d) surface + VSP images. The receivers depth of surface observation system is z = 100 m. The receivers positions of VSP observation system are x = 10 m and x = 4990 m, respectively, as denoted by yellow vertical lines.

RTMs. The developed schemes can produce high modeling and imaging accuracy, as demonstrated by several numercial examples.

#### Acknowledgements

This research is supported by the National Key R&D Program of China (2021YFA0716902), National Natural Science Foundation of China (42004119, 42174156), the Fundamental Research Funds for the Central Universities, CHD (300102261306), and the National Engineering Research Center of Offshore Oil and Gas Exploration, No. 6 Courtyard, Taiyanggong South Street, Chaoyang District, Beijing, 100028.

#### Appendix A

In this section, we briefly introduce the implementation procedures of Poisson algorithm from the following steps (Li and Zhu, 2018):

(1) Adopting five-points FD to approximate Eq. (11),

$$U_{j-1,l}^{o} + U_{j+1,l}^{o} + U_{j,l-1}^{o} + U_{j,l+1}^{o} - 4U_{j,l}^{o} = h^{2}P_{j,l}^{o},$$
(36)

where *h* is the grid spacing.

(2) Using forward sine transform to calculate the Fourier response  $\hat{P}$  of wavefield component P:

$$\hat{P}_{i,k} = \frac{1}{L_x L_z} \sum_{i=1}^{L_x - 1} \sum_{l=1}^{L_z - 1} P_{j,l}^o \sin\left(\frac{-jk\pi}{L_x}\right) \sin\left(\frac{-lk\pi}{L_z}\right),\tag{37}$$

where  $L_x$  and  $L_z$  are spatial grid dimensions along x and z directions.

(3) Based on the step (2), compute the Fourier response of the auxiliary wavefield *U* as follow:

$$\hat{U}_{i,k} = \frac{\hat{P}_{i,k}}{\lambda_{i,k}}, \quad \lambda_{i,k} = 4 - 2\cos\left(\frac{i\pi}{L_x}\right) - 2\cos\left(\frac{k\pi}{L_z}\right). \tag{38}$$

(4) By combining the Fourier response  $\hat{U}$ , wavefield U can be generated by the following inverse sine transform:

$$(36) U_{j,l} = \sum_{i=1}^{L_x - 1} \sum_{k=1}^{L_z - 1} \hat{U}_{i,k} \sin\left(\frac{jk\pi}{L_x}\right) \sin\left(\frac{lk\pi}{L_z}\right). (39)$$

#### References

- Alkhalifah, T., 1998. Acoustic approximations for processing in transversely isotropic media. Geophysics 63 (2), 623–631. https://doi.org/10.1190/1.1444361.
- Alkhalifah, T., 2013. Residual extrapolation operators for efficient wavefield construction. Geophys. J. Int. 193 (2), 1027–1034. https://doi.org/10.1093/gji/ggt040.
- Baysal, E., Kosloff, D., Sherwood, J.W., 1983. Reverse time migration. Geophysics 48 (11), 1514–1524. https://doi.org/10.1190/1.1441434.
- Bai, J., Yingst, D., Bloor, R., et al., 2014. Viscoacoustic waveform inversion of velocity structures in the time domain. Geophysics 79 (3), R103—R119. https://doi.org/ 10.1190/GF02013-0030.1.
- Bai, T., Tsvankin, I., 2016. Time-domain finite-difference modeling for attenuative anisotropic media. Geophysics 81 (2), C69–C77. https://doi.org/10.1190/ CF0.2015-0424.1
- Blanch, J., Robertsson, J., Symes, W., 1995. Modeling of a constant Q: methodology and algorithm for an efficient and optimally inexpensive viscoelastic technique. Geophysics 60 (1) 176–184. https://doi.org/10.1190/1.1443744
- Geophysics 60 (1), 176–184. https://doi.org/10.1190/1.1443744.
  Blanc, E., Komatitsch, D., Chaljub, E., 2016. Highly accurate stability-preserving optimization of the Zener viscoelastic model, with application to wave propagation in the presence of strong attenuation. Geophys. J. Int. 205 (1), 427–439. https://doi.org/10.1093/gji/ggw024.
- Carcione, J.M., 1992. Anisotropic Q and velocity dispersion of finely layered media. Geophys. Prospect. 40, 761–783. https://doi.org/10.1111/j.1365-2478.1992.tb00551.x.
- Carcione, J.M., 1995. Constitutive model and wave equations for linear, viscoelastic, anisotropic media. Geophysics 60, 537–548. https://doi.org/10.1190/1.1443791.
- Carcione, J.M., Cavallini, F., Mainardi, F., et al., 2002. Time-domain modeling of constant-Q seismic waves using fractional derivatives. Pure Appl. Geophys. 159 (7), 1719–1736. https://doi.org/10.1007/s00024-002-8705-z.
- Carcione, J.M., Kosloff, D., Kosloff, R., 1988. Wave propagation simulation in a linear viscoacoustic medium. Geophys. J. Int. 93, 393–401. https://doi.org/10.1111/ j.1365-246X.1988.tb02010.x.
- Chen, B., Jia, X., 2014. Staining algorithm for seismic modeling and migration. Geophysics 79 (4), S121–S129. https://doi.org/10.1190/GEO2013-0262.1.
- Chen, H., Zhou, H., Li, Q., et al., 2016. Two efficient modeling schemes for fractional Laplacian viscoacoustic wave equation. Geophysics 81 (5), T233—T249. https://doi.org/10.1190/GEO2015-0660.1.
- Chu, C., Macy, B.K., Anno, P.D., 2011. Approximation of pure acoustic seismic wave propagation in TTI media. Geophysics 76 (5), WB97—WB107. https://doi.org/ 10.1190/GEO2011-0092.1.
- Du, X., Bancroft, J.C., Lines, L.R., 2007. Anisotropic reverse-time migration for tilted TI media. Geophys. Prospect. 55 (6), 853–869. https://doi.org/10.1111/j.1365-2478.2007.00652.x.
- Duveneck, E., Bakker, P.M., 2011. Stable P-wave modeling for reverse-time migration in tilted TI media. Geophysics 76 (2), S65—S75. https://doi.org/10.1190/1.3533964.
- Fletcher, R.P., Du, X., Fowler, P.J., 2009. Reverse time migration in tilted transversely isotropic (TTI) media. Geophysics 74 (6), WCA179–WCA187. https://doi.org/10.1100/1.3269002
- Fomel, S., Ying, L., Song, X., 2013. Seismic wave extrapolation using lowrank symbol approximation. Geophys. Prospect. 61, 526–536. https://doi.org/10.1111/j.1365-2478.2012.01064.x
- Hao, Q., Alkhalifah, T., 2019. Viscoacoustic anisotropic wave equations. Geophysics 84 (6), C323–C337. https://doi.org/10.1190/GEO2018-0865.1.
- Kjartansson, E., 1979. Constant Q-wave propagation and attenuation. J. Geophys. Res. 84, 4737–4748. https://doi.org/10.1029/JB084iB09p04737.
- Koene, E.F., Robertsson, J.O., Broggini, F., et al., 2018. Eliminating time dispersion from seismic wave modeling. Geophys. J. Int. 213, 169–180. https://doi.org/ 10.1093/gji/ggx563.
- Li, J., Xin, K., Dzulkefli, F.S., 2022. A new qP-wave approximation in TTI media and its reverse time migration for areas with complex overburdens. Geophysics 87 (4), \$237-\$248. https://doi.org/10.1190/geo2021-0433.1.
- Li, X., Zhu, H., 2018. A finite-difference approach for solving pure quasi-p-wave equations in transversely isotropic and orthorhombic media. Geophysics 83 (4), C161—C172. https://doi.org/10.1190/GEO2017-0405.1.
- Liu, F., Morton, S.A., Jiang, S., et al., 2009. Decoupled wave equations for P and SV

- waves in an acoustic VTI media. 79th Ann. Int. Meet. SEG, Expand. Abstr. 2844–2848, https://doi.org/10.1190/1.3255440.
- Liu, Y., Chang, X., Jin, D., et al., 2011. Reverse time migration of multiples for subsalt imaging. Geophysics 76 (5), WB209—WB216. https://doi.org/10.1190/GEO2010-0312.1
- McMechan, G., 1983. Migration by extrapolation of time-dependent boundary values. Geophys. Prospect. 31 (3), 413–420. https://doi.org/10.1111/j.1365-2478.1983.tb01060.x.
- Mu, X., Huang, J., Yong, P., et al., 2020. Modeling of pure qP-and qSV-waves in tilted transversely isotropic media with the optimal quadratic approximation. Geophysics 85 (2). C71—C89. https://doi.org/10.1190/GEO2018-0460.1.
- Mu, X., Huang, J., Yang, J., et al., 2022. Modeling of Pure visco-qP-wave propagation in attenuating tilted transversely isotropic (TTI) media based on decoupled fractional Laplacians. Geophysics 87 (4), T291–T313. https://doi.org/10.1190/ GEO2021-0440.1.
- Pestana, R.C., Ursin, B., Stoffa, P., 2011. Separate P- and SV-wave equations for VTI media. 81th Ann. Int. Meet. SEG, Expand. Abstr. 163–167. https://doi.org/10.1190/1.3627518.
- Shi, Y., Wang, Y., 2016. Reverse time migration of 3D vertical seismic profile data. Geophysics 81 (1), S31–S38. https://doi.org/10.1190/GEO2015-0277.1.
- Song, L., Shi, Y., Chen, S., et al., 2021. Target-oriented reverse time migration in transverse isotropy media. Acta Geophys. 69 (1), 125–134. https://doi.org/10.1007/s11600-020-00527-9.
- Sun, J., Zhu, T., Fomel, S., 2015. Viscoacoustic modeling and imaging using low-rank approximation. Geophysics 80 (5), A103—A108. https://doi.org/10.1190/
- Sun, B., Alkhalifah, T., 2021. Pseudoelastic pure P-mode wave equation. Geophysics 86 (6), T469–T485. https://doi.org/10.1190/GEO2021-0084.1.
- Thomsen, L., 1986. Weak elastic anisotropy. Geophysics 51 (10), 1954–1966. https://doi.org/10.1190/1.1442051.
- Tsvankin, I., 1996. P-wave signatures and notation for transversely isotropic media: an overview. Geophysics 61 (2), 467–483. https://doi.org/10.1190/1.1443974.
- Wang, E., Liu, Y., Ji, Y., et al., 2019. Q full-waveform inversion based on the viscoacoustic equation. Appl. Geophys. 16 (1), 77–91. https://doi.org/10.1007/s11770-019-0749-2
- Xing, G., Zhu, T., 2019. Modeling frequency-independent Q viscoacoustic wave propagation in heterogeneous media. J. Geophys. Res. 124 (11), 11568–11584. https://doi.org/10.1029/2019JB017985.
- Yang, J., Zhu, H., 2018. A time-domain complex-valued wave equation for modelling visco-acoustic wave propagation. Geophys. J. Int. 215 (2), 1064–1079. https:// doi.org/10.1093/gji/ggy323.
- Yuan, S., Wang, S., Tian, N., et al., 2016. Stable inversion-based multitrace deabsorption method for spatial continuity preservation and weak signal compensation. Geophysics 81 (3), V199–V212. https://doi.org/10.1190/GEO2015-0247.1.
- Zhan, G., Pestana, R.C., Stoffa, P.L., 2012. Decoupled equations for reverse time migration in tilted transversely isotropic media. Geophysics 77 (2), T37–T45. https://doi.org/10.1190/GEO2011-0175.1.
- Zhang, H., Zhang, Y., 2008. Reverse time migration in 3D heterogeneous TTI media. 78th Ann. Int. Meet. SEG, Expand. Abstr. 2196–2200. https://doi.org/10.1190/
- Zhang, Y., Liu, Y., Xu, S., 2019. Efficient modelling of optimised pure acoustic wave equation in 3D transversely isotropic and orthorhombic anisotropic media. Explor. Geophys. 50 (5), 561–574. https://doi.org/10.1080/08123985.2019.1643680.
- Zhou, H., Zhang, G., Bloor, R., 2006. An anisotropic acoustic wave equation for modeling and migration in 2D TTI media. 76th Ann. Int. Meet. SEG, Expand. Abstr. 194–198. https://doi.org/10.1190/1.2369913.
- Zhou, T., Hu, W., Ning, J., 2020. Broadband Finite-difference Q-RTM algorithm for TTI media. Geophysics 85 (5), S241–S253. https://doi.org/10.1190/geo2018-0862.1.
- Zhu, T., Bai, T., 2019. Efficient modeling of wave propagation in a vertical transversely isotropic attenuative medium based on fractional Laplacian. Geophysics 84 (3), T121–T131. https://doi.org/10.1190/GEO2018-0538.1.
- Zhu, T., Harris, J., 2014. Modeling acoustic wave propagation in heterogeneous attenuating media using decoupled fractional Laplacians. Geophysics 79 (3), T105–T116. https://doi.org/10.1190/GEO2013-0245.1.
- Zhu, T., Harris, J., Biondi, B., 2014. Q-compensated reverse-time migration. Geophysics 79 (3), S77–S87. https://doi.org/10.1190/GEO2013-0344.1.